Powder Metallurgy and Metal Ceramics, Vol. 52, Nos. 9-10, January, 2014 (Russian Original Vol. 52, Nos. 9-10, Sept.-Oct., 2013)

NANOSTRUCTURED MATERIALS

PRODUCTION AND PROPERTIES OF NANOSTRUCTURED METAL-OXIDE LEAD ZIRCONATE–TITANATE PIEZOCERAMICS

V. V. Prisedskii,[1,2] V. M. Pogibko,[1] and V. S. Polishchuk[1]

UDC 621.762+546.831+541.4

Compact ceramic samples of lead zirconate–titanate are sintered from nanocrystalline (d_{av} = = 25 nm) $Pb(Zr_{0.52}Ti_{0.48})O_3$ powder synthesized by thermal decomposition of an oxalate precursor. Conditions of nanopowder compaction have been found and kinetics of sintering and growth of nanocrystallites and coarser grains formed during consolidation have been studied. The lead zirconate–titanate ceramic samples consolidated from nanopowders are sintered at lower (by 300–350°C) temperatures and have higher (by 25–45%) dielectric and piezoelectric properties as compared to samples fabricated by conventional solid-state technology. Two-level grain structure is formed during sintering: nanocrystallites divided by low-angle boundaries and descending from initial nanocrystalline particles and consolidated coarser micrograins divided by high-angle boundaries. Sintering of the lead zirconate–titanate ceramics from nanocrystalline powders permits controlling the nanoscale size of crystallites and thus the nanostructured features of consolidated material.

Keywords*: sintering, consolidation, nanocrystalline powder, piezoceramics, lead zirconate–titanate, electrophysical properties.*

INTRODUCTION

Power metallurgy methods are often used for consolidating nanocrystalline powders into solid articles. This paper considers the production and properties of consolidated nanostructured lead zirconate–titanate (PZT) piezoceramics.

Lead zirconate–titanate solid solutions [1] possess excellent electrophysical properties and have formed the basis for the most popular ferro- and piezoceramics. They show noncentrosymmetrical perovskite structure below the Curie point, T_C, and many of their properties have a maximum near the morphotropic phase boundary (close to the composition $Pb(Ti_{0.48}Zr_{0.52})O_3$), where the elementary cell transforms from tetragonal to rhombohedral lattice distortion when the Ti/Zr ratio changes. Other factors influencing the properties of PZT include composition and concentration of modifying (doping) additions, deviations from stoichiometry, density and porosity of ceramic articles, sizes of grains and crystallites, characteristics of raw materials, and features of production methods.

[1]Donetsk National Technical University, Scientific and Technological Center Reaktivelektron, National Academy of Sciences of Ukraine, Donetsk.

[2]To whom correspondence should be addressed; e-mail: prisedskyvadim@mail.ru.

Translated from Poroshkovaya Metallurgiya, Vol. 52, No. 9–10 (493), pp. 24–35, 2013. Original article submitted December 4, 2012.

The potential to improve the properties of PZT ferro- and piezoceramics by complicating their composition and choosing the optimum sintering conditions [2] has practically been exhausted. Research attention is currently focused on prospects of making nanocrystalline materials as well as consolidated nanostructured bulk and film articles [3]. Ceramic synthesis is a conventional method of producing PZT piezoceramics [4]. To make nanocrystalline perovskite oxides, high-energy mechanical alloying [5], laser deposition [6], various solution chemistry techniques [7–11], such as codeposition, hydrothermal synthesis, and sol-gel process, thermolysis and combustion of precursors [12–15], and other methods are employed.

The properties of nanoparticles show a more pronounced dependence on the size of crystallites than those of coarser particles. The ferroelectric Curie point, T_C, of nonconsolidated nanocrystalline powders of $BaTiO_3$ and other perovskite oxides decreases with smaller crystallites, indicating that the ferroelectric state is suppressed. The relaxor nature of the temperature dependence for permittivity ε enhances in the same direction. According to Raman spectroscopy [9], the morphotropic phase boundary shifts in PZT at $d < 100$ nm. An fcc phase shows up in nanocrystalline PZT, while it is not found in micro- and macropowders [13].

Much fewer studies deal with the properties of consolidated nanostructured PZT ceramics. The $Pb(Ti_{0.47}Zr_{0.53})O_3$ samples produced by the sol-gel method and consolidated by sintering are characterized by increasing relative permittivity $\varepsilon/\varepsilon_0$ when crystallites decrease from 150 to 40 nm [5]. The paper [16] studied the main ferroelectric and piezoelectric properties of $Pb(Ti_{0.50}Zr_{0.50})O_3$ samples hot-pressed from nanocrystalline powders with an average particle size of 30 nm at $\varepsilon/\varepsilon_0$ (300 K) = 1100, residual polarization $P_R = 0.25$ C/m^2, piezoelectric coupling coefficient $k_p = 0.5$, and piezoelectric modulus $d_{33} = 180$ pC/N [16].

In this study, we consolidated the nanocrystalline powder to make compact $Pb(Zr_{0.52}Ti_{0.48})O_3$ piezoceramics, studied the conditions and kinetics of sintering, recrystallization growth of grains, and electrophysical properties of the samples.

EXPERIMENTAL

Nanocrystalline PZT powders were synthesized through thermal decomposition of an oxalate precursor [17–19]. Following more than 50 years after Clabaugh's groundbreaking study [17], the full sequence of transformations and the composition of intermediate amorphous products formed in the synthesis of perovskite phases when oxalate precursors thermally decompose are still open to question. We compared quantitative results of gravimetric analyses for the thermal decomposition of oxalate complexes of titanium and zirconium with data for a series of individually synthesized potential intermediate products of decomposition and determined quite a detailed scheme of thermolysis reactions [19]; this allowed us to clarify possible ways to synthesize nanocrystalline perovskite phases at lower temperatures.

The starting reagents were titanium tetrachloride $TiCl_4$ (extra-pure grade), zirconium oxychloride $ZrOCl_2 \times \times 8H_2O$ (chemically pure), lead nitrate $Pb(NO_3)_2$ (chemically pure), ammonia NH_3 (25% aqueous solution, chemically pure), oxalic acid $H_2C_2O_4 \cdot 2H_2O$ (chemically pure), ammonium oxalate $(NH_4)_2C_2O_4 \cdot H_2O$ (chemically pure), and bidistillate H_2O.

To synthesize PZT oxalate precursors, we first introduced the aqueous ammonia solution (4.4–4.5 M) to precipitate titanium and zirconium hydroxides from chloride solutions (2–2.1 M) in the following molar ratio:

$$0.48TiCl_4 + 0.52ZrOCl_2 + 2.96NH_3 + 2.48H_2O \rightarrow H_2(Ti_{0.48}Zr_{0.52})O_3 \downarrow + 2.96NH_4Cl.$$

The wet precipitate (85–90% water) was washed in distilled water using a Buchner funnel under vacuum until chloride ions were no longer present ($AgNO_3$ test), repulped in distilled water (S : L = 2 : 1), heated to 50–60°C, and dissolved in a 2M oxalic acid solution, to be further neutralized with ammonia to pH = 2.5 at 60°C:

$$H_2(Ti_{0.48}Zr_{0.52})O_3 + 2H_2C_2O_4 \rightarrow H_2[(Ti_{0.48}Zr_{0.52})O(C_2O_4)_2] + 2H_2O;$$

$$H_2[(Ti_{0.48}Zr_{0.52})O(C_2O_4)_2] + 2NH_3 \rightarrow (NH_4)_2[(Ti_{0.48}Zr_{0.52})O(C_2O_4)_2].$$

The resultant solution was filtered, and then a 1.5M lead nitrate solution was added at 80°C with vigorous stirring, pH being kept at 4–5:

$$(NH_4)_2[(Ti_{0.48}Zr_{0.52})O(C_2O_4)_2] + Pb(NO_3)_2 + 4H_2O \rightarrow 2NH_4NO_3 + Pb[(Ti_{0.48}Zr_{0.52})O(C_2O_4)_2] \cdot 4H_2O \downarrow.$$

The precipitate was filtered and washed with distilled water on a vacuum filter, and the PZT oxalate precursor—lead tetrahydrate titanate–zirconate dioxalate—was dried at 120°C and in 0.7 MPa vacuum.

Nanocrystalline PZT powder was produced through thermal decomposition of the oxalate precursor. The temperature range and amount of the fine perovskite phase are known to be largely dependent on the heating rate in polythermal mode [18]. We preliminary analyzed kinetics of the process and accepted the following procedure to synthesize nanocrystalline PZT.

An alundum crucible with a 4-mm layer of the oxalate precursor powder was placed into a KO-14 furnace with silit heaters. The heat treatment included heating to 370°C at a rate of 15°C/min, isothermal holding at 370°C for 45 min, rapid heating in a high-gradient field from 370 to 750°C, holding for 45 min at a maximum temperature of 750°C, and cooling with the furnace.

X-ray diffraction patterns of the samples were taken with a DRON-3 diffractometer in filtered Cu-K_α radiation. The diffraction patterns were identified using ASTM files. The average size d_{av} of crystallites (coherent scattering domains, CSDs) was calculated by the Scherrer equation:

$$\langle d_c \rangle = \frac{K_{hkl}\lambda}{\beta \cdot 2\cos\theta},$$

where K_{hkl} is the Scherrer constant; λ is the X-ray wavelength; β is true physical broadening of the diffraction peak at half height; θ is the reflection angle.

The morphology and size of powder particles were examined with a JEOL JEM 200A transmission electron microscope (TEM) and a JEOL TSM-T30 scanning electron microscope (SEM). The specific surface area of the powders was determined by multilayer adsorption (BET) of argon using a SoftSorbi-II device. The curves showing shrinkage during sintering were plotted with a DIL 402 PC dilatometer.

The dielectric properties (capacity, conductivity, and dielectric losses tgδ) of the powders and ceramics samples were analyzed with an E7-8LCR meter at 1 kHz and output voltage lower than 1 V. The piezoelectric properties were measured by resonance–antiresonance on 10 mm × 1 mm disk samples at 1 kHz. The samples were polarized in polyethylsiloxane fluid in a 4 kV/mm filed at 120–150°C for 30 min and then cooled in the field to room temperature.

RESULTS AND DISCUSSION

Figure 1 shows electron microscopy (TEM) images of the synthesized nanocrystalline PZT powder. The particles are quite uniform in size; their average size (secant method) is d_{av} = 23 nm and the shape is close to polyhedral in most instances. The photograph in Fig. 1*b*, taken from a substantial amount of powder on the substrate, illustrates significant adhesion between particles in nanocrystals.

According to XRD, the synthesized material is single-phase perovskite. The average size of crystallites (CSDs) measured from broadening of <111> and <200> reflections is 25 nm, which practically agrees with the TEM results.

The synthesized powder was used to form and sinter 10 mm × (1–1.5) mm ceramic disks. It has been found that the fine and uniform size as well as strong adhesion between particles substantially hinder the formation of nanocrystalline samples. The compaction curves (Fig. 2) show that total porosity θ of the nanocrystalline powder pressed without a binder at 300 MPa remains above 45%, two times as high as that of the microcrystalline powder synthesized conventionally. Such compacts are brittle. To obtain good results, liquid binders based on surfactants had to be selected to promote sliding and rotation of nanocrystallites and increase compacting pressure to 600 MPa. The best results were obtained when a complex binder based on dibutyl sebacate (DBS) and polyvinyl butyral (PVB) solutions in acetone was used.

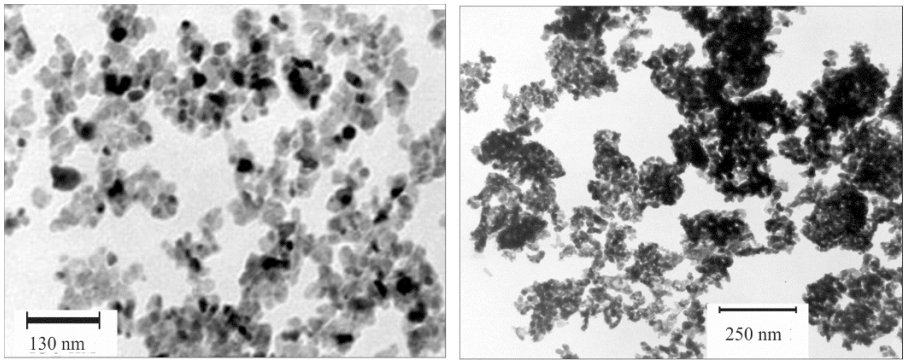

a *b*

Fig. 1. Electron microscopy (TEM) images of the nanocrystalline PZT powder synthesized from the oxalate precursor

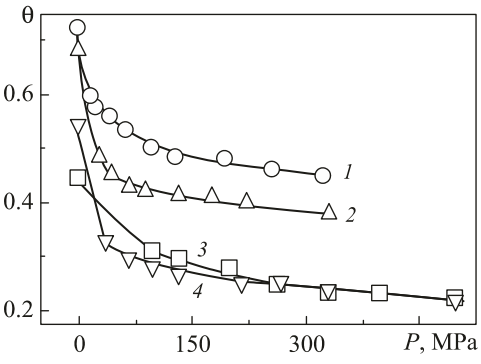

Fig. 2

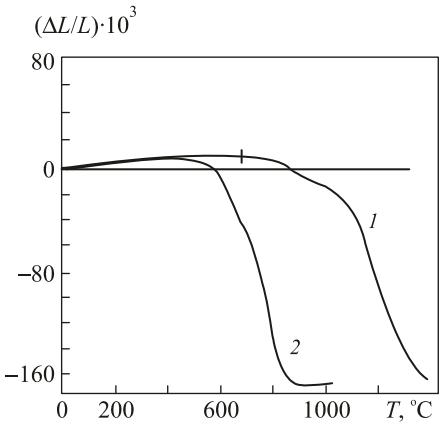

Fig. 3

Fig. 2. Compaction curves for nanocrystalline (*1*, *2*) and microcrystalline (*3*, *4*) PZT powders: *1*, *3*) without binder; *2*, *4*) with DBS + PVB binder

Fig. 3. Dilatometric curves for PZT sintering at a heating rate of 10ºC/min: *1*) conventional ceramic method; *2*) nanocrystalline powder from the oxalate precursor

The dilatometric curves showing shrinkage of powder compacts (Fig. 3) indicate that the sintering temperature of the nanocrystalline PZT powder is much lower than that of the conventional powder. At a heating rate of 10°C/min in polythermal mode, the shrinkage of nanocrystalline PZT compacts is completed below 900°C, i.e., at a temperature 300 to 350°C lower than for conventional ceramic samples.

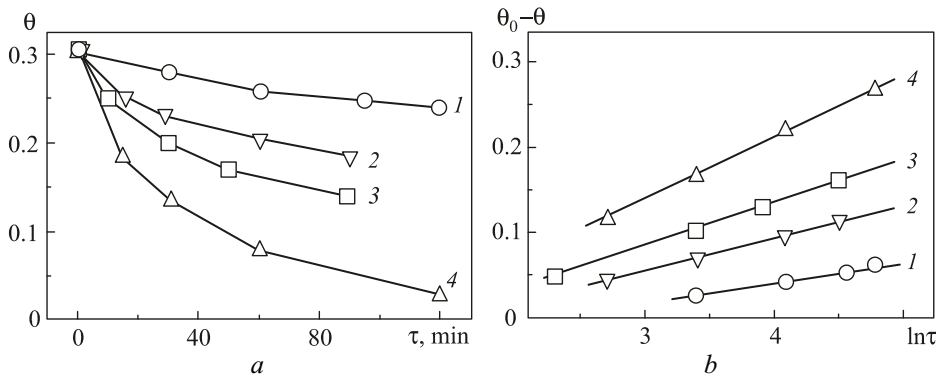

a *b*

Fig. 4. Densification kinetics of the nanocrystalline PZT powder in direct (*a*) and semilogarithmic (*b*) coordinates: *T* = 700 (*1*), 750 (*2*), 800 (*3*), and 850°C (*4*)

The isothermal kinetics of pressureless sintering (Fig. 4) was studied in the range 700–850°C, the bulk density of compacts being measured after different times of isothermal holding. Total residual porosity θ was calculated by comparing the measured and X-ray bulk density.

Even within 1.5 h of sintering at 850°C, the total residual porosity of the samples decreases to a few percent (Fig. 4*a*), i.e., to the value typical of high-quality PZT piezoceramic samples after pressureless sintering. The kinetic curves of densification were linearized in semilogarithmic coordinates (Fig. 4*b*) to show that the porosity can be described as

$$\theta_0 - \theta = B(T)\ln\tau = \frac{N \cdot \sigma \cdot D \cdot a^3}{A \cdot kT} \cdot \ln\tau, \tag{1}$$

which was proposed by Coble [22] for the densification model with bulk diffusion in the transient and final sintering periods accompanied by simultaneous grain growth by cubic law:

$$d_g^3 - d_{g(0)}^3 = A(T) \cdot \tau, \tag{2}$$

where N is a numerical coefficient ($N = 10$ for the intermediate stage (connected pores) and $N = 3\pi$ for the final stage (isolated pores) of sintering); σ is surface tension; D is the diffusion coefficient; a is the lattice parameter; d_g and $d_{g(0)}$ are the current and initial grain sizes. The apparent activation energy for densification during sintering of the nanocrystalline powder compact is $E_A = 75 \pm 4$ kJ/mol (versus 140 kJ/mol for conventional sintering of ceramic compacts) [21].

Compaction of nanocrystalline powders opens the way to reduce their high surface energy through reorientation of adjacent particles (partly during pressing) and to promote much coarser grain structures in which starting crystallites are reoriented in a correlated manner [23]. Electron microscopy (SEM) analyses show (Fig. 5) that these processes are accelerated in the temperature range of sintering to lead to the formation and subsequent growth of microcrystalline grain structure. Note that microcrystalline grains do not result from normal growth of the starting nanocrystalline particles but rather from their reorientation and association.

Finally, the microstructure of sintered samples shows nanosized crystallites (d_c) divided by low-angle boundaries and descending from the starting nanocrystalline particles and submicro- and even microsized grains (d_g) divided by high-angle boundaries. The nanosized crystallites are experimentally identified as CSDs. For convenience, we will further refer to the former as crystallites and to the latter as grains.

Individual nanosized crystallites (CSDs) inside the grains partly retain their features and can grow with increasing temperature. However, the growth kinetics of crystallites and grains is different (Fig. 6).

In the initial sintering stage (at 850°C), the average size of crystallites, d_c, rapidly (within 30 min) changes from initial 25 nm to 45 nm; their growth dramatically slows down during further holding unlike the microsized grains (d_g).

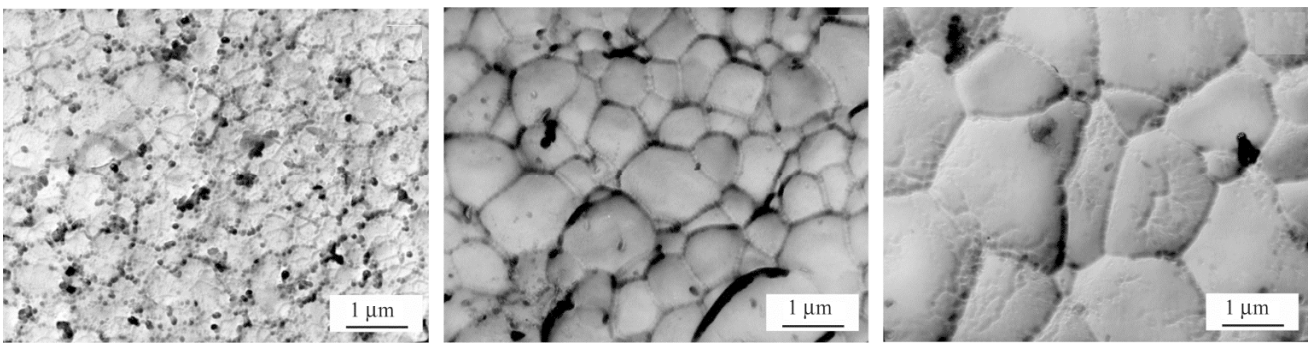

a *b* *c*

Fig. 5. Formation and growth of microcrystalline grains during sintering of nanocrystalline PZT powder at 850°C and holding time of 30 (*a*), 60 (*b*), and 180 (*c*) min

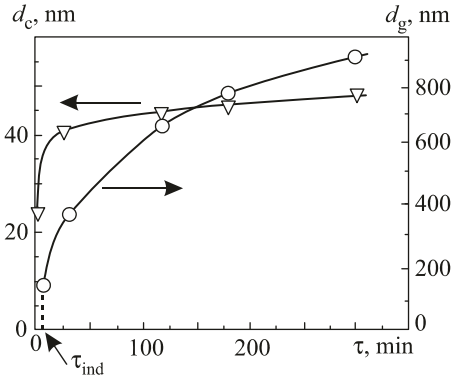

Fig. 6. Growth kinetics of grains d_g and crystallites d_c during sintering of the nanocrystalline PZT powder at 850°C

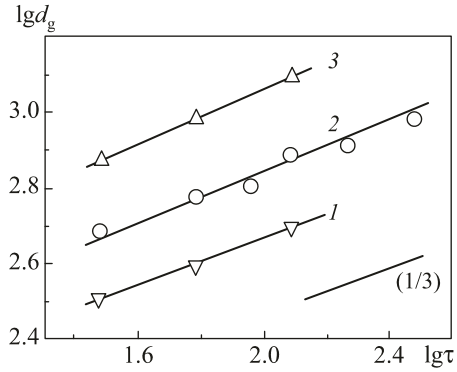

Fig. 7. Grain growth kinetics for nanostructured PZT ceramics in logarithmic coordinates: T = 750 (*1*), 850 (*2*), and 950°C (*3*)

TABLE 1. Kinetic Parameters of Grain Growth and Densification during Sintering of Nanocrystalline PZT Powder

Parameter	Temperature, °C				
	700	750	800	850	950
Parameter A in Eq. (2), $A \cdot 10^{23}$, m^3/sec	–	2.39 ± 0.03	–	8.18 ± 0.16	15.2 ± 0.18
Grain growth activation energy, kJ/mol			106 ± 12		
Parameter B in Eq. (1), $B \cdot 10^2$	2.42 ± 0.19	3.84 ± 0.22	5.02 ± 0.16	7.50 ± 0.12	–
Compaction activation energy, kJ/mol			75 ± 4		
Diffusion coefficient $D \cdot 10^{17}$, m^2/sec	0.74 ± 0.06	1.2 ± 0.08	3.4 ± 0.2	8.9 ± 0.3	–
Diffusion activation energy E_A, kJ/mol			188 ± 15		

Hence the actual advantage of using nanocrystalline powders to produce PZT ceramics is that the nanosize of crystallites (CSDs) and thus the nanostructure of consolidated material can be controlled.

It follows from the slopes of curves in double logarithmic coordinates (Fig. 7) that the kinetics of grain growth in the range 750–950°C obeys the power law with exponent 1/3, corresponding (for small $d_{g(0)}$) to the model of growth through bulk diffusion [22] by Eq. (2).

Table 1 shows experimental kinetic parameters for growth of grains and sintering of ceramic PZT compacts. The activation energies of grain growth and densification were calculated from temperature dependences

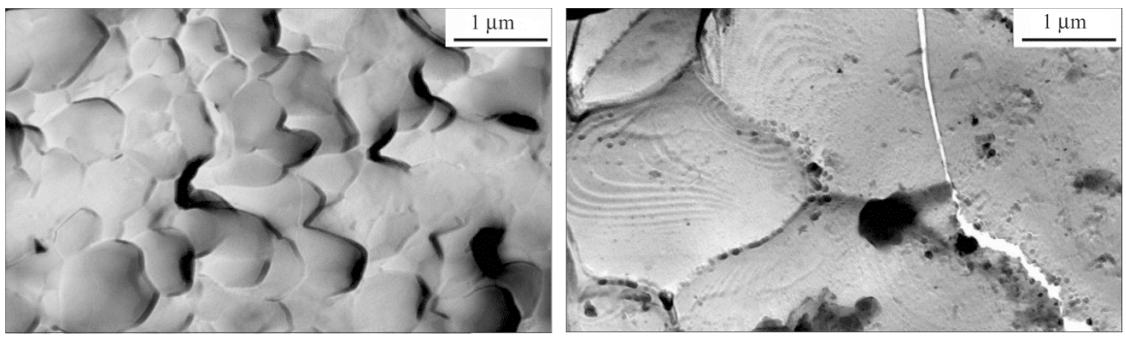

a *b*

Fig. 8. Grain microstructure of sintered PZT ceramics: *a)* ceramics consolidated from nanosized powder; *b)* conventional synthesis and sintering

TABLE 2. Electrophysical Properties of $Pb(Zr_{0.52}Ti_{0.48})O_3$ Piezoceramics Produced from Nanocrystalline Powder (NP) and by Conventional Method (CM)

Samples and microstructural parameters	$\varepsilon_{33}/\varepsilon_0$	tgδ	K_p	Q_m	d_{31}, pC/N	d_{33}, pC/N	T_C, °C
CM, d_g = 7 μm, d_c = 200 nm	760 ± 70	0.004	0.52	500	90 ± 7	220 ± 15	385
NP, d_g = 0.65 μm, d_c = 45 nm	1100 ± 60	0.003	0.54	650	120 ± 5	270 ± 10	385

$A(T)$ and $B(T)$. The diffusion coefficients D of particles limiting the rate of transfer during sintering were calculated using $B(T)$ by Eq. (1) (PZT surface tension was $\sigma = 1.6$ J/m^2).

The magnitudes of calculated D and E_A are close to the parameters of self-diffusion of lead cations in PZT and substantially differ, by many orders, from the parameters of diffusion of oxygen and small cations (Zr and Ti) in PZT [2, 21].

Figure 8 compares typical diffraction patterns (SEM images) for fractured surfaces of PZT ceramics sintered from the nanocrystalline powder at 850°C for 1 h ($d_g = 0.65$ μm, $d_c = 45$ nm) and PZT ceramics conventionally sintered from microcrystalline powder at 1250°C for 1 h ($d_g = 7$ μm, $d_c = 200$ nm). The images demonstrate the advantages of nanostructured ceramics. The PZT ceramics produced conventionally (Fig. 8*b*) show a wide grain-size distribution and have visible pores inside and between the grains. The PZT ceramics sintered from the nanocrystalline powder (Fig. 8*a*) have submicron grain structure and show more uniform grain-size distribution and dense grain boundaries, practically without pores.

Table 2 shows that the electrophysical properties of $Pb(Zr_{0.52}Ti_{0.48})O_3$ ceramics consolidated from nanocrystalline powders (NP) are much higher than those of the ceramics produced with conventional method: by 25–30% for piezoelectric moduli d_{31} and d_{33} and by 45% for relative permittivity. The piezoelectric coupling coefficient K_p, mechanical quality factor Q_m, and dielectric losses tgδ improve as well.

The high dielectric and piezoelectric properties of PZT ceramics produced from nanocrystalline powders ascertain that nanosized crystallites within one microcrystalline grain are connected: their low-angle boundaries do not prevent atomic vibrations from assembling within a single ferroelectric domain. That is why the consolidated ceramics differ from a mixture of free nanocrystallites, where reduction in the particle size decreases the Curie point and suppresses ferroelectric properties. At the same time, local mechanical stresses on the developed interfaces of nanocrystallites (in particular, dislocations and disclinations) may lead to pseudomorphotropic domains, facilitate the movement of domain walls, reorient polarization, and improve associated electrophysical properties. The interfaces are more developed in the PZT ceramics consolidated from nanocrystalline powder than in conventionally sintered samples.

CONCLUSIONS

Compact ceramic samples of lead zirconate–titanate (PZT) are sintered from nanocrystalline $Pb(Zr_{0.52}Ti_{0.48})O_3$ powder ($d_{av} = 25$ nm) at temperatures lower by 300–350°C than conventional ceramic samples. To make nanopowders, liquid binders based on surfactants were selected to promote sliding and rotation of nanocrystallites in compacts. The sintering and grain growth kinetics corresponds to the model with bulk diffusion in the transient and final sintering periods accompanied by simultaneous grain growth by cubic law.

Consolidation of the nanocrystalline powder during sintering leads to much coarser (micron) grains. The latter do not result from normal diffusion-controlled growth of the starting nanocrystalline particles but from the association of many (10^3–10^4) crystallites under the action of high surface energy, which changes their orientation in a correlated manner through slipping and rotation. The resultant ceramics have two-level grain structure: nanosized crystallites divided by low-angle boundaries and descending from nanocrystalline powder particles and

microcrystalline grains divided by high-angle boundaries. The use of nanocrystalline powder to make PZT ceramics allows the nanosize of crystallites to be controlled, thus promoting nanostructured consolidated material.

The differences in the size ratio of crystallites (CSDs) and grains divided by high-angle boundaries lead to better dielectric and piezoelectric properties of the PZT ceramics compared to conventionally synthesized samples.

REFERENCES

1. B. Jaffe, R. S. Roth, and S. Marzullo, "Piezoelectric properties of lead zirconate–lead titanate solid-solution ceramics," *J. Appl. Phys.*, **25**, No. 6, 809–810 (1954).
2. V. V. Prisedskii, *Nonstoichiometric Ferroelectrics* $A^{II}B^{IV}O_3$ [in Russian], Knowledge, Donetsk (2011), p. 267.
3. M. D. Glinchuk and A. V. Ragulya, *Nanoferroics* [in Russian], Naukova Dumka, Kiev (2009), p. 275.
4. Y. Matsuo and H. Sasaki, "Formation of lead zirconate–lead titanate solid solutions," *J. Am. Ceram. Soc.*, **48**, 289–291 (1965).
5. B. Praveenkumar, G. Sreenivasalu, H. H. Kumar, et al., "Size effect studies on nanocrystalline $Pb(Zr_{0.53}Ti_{0.47})O_3$ synthesized by mechanical activation route," *Mater. Chem. Phys.*, **117**, 338–342 (2009).
6. F. Craciun, M. Dinescu, P. Verardi, and C. Galassi, "Pulsed laser deposition of nanocrystalline lead zirconate–titanate thin films," *Nanotechnology*, **10**, 81–85 (1999).
7. Q. F. Zhou, H. L. W. Chan, and C. L. Choy, "Nanocrystalline powders and fibers of lead zirconate–titanate prepared by the sol-gel process," *J. Mater. Process. Technol.*, **63**, 281–285 (1997).
8. Y. Faheem and M. Shoaib, "Sol-gel processing and characterization of phase-pure lead zirconate–titanate nanopowders," *J. Am. Ceram. Soc.*, **89**, No. 6, 2034–2037 (2006).
9. J. F. Meng, "Raman phonon modes and ferroelectric phase transitions in nanocrystalline lead zirconate–titanate," *Phys. Stat. Sol. (A)*, **164**, 851–862 (1997).
10. G. Garnweitner, J. Hentschel, M. Antonietti, and M. Niederberger, "Nonaqueous synthesis of amorphous powder precursors for nanocrystalline $PbTiO_3$, $Pb(Zr,Ti)O_3$, and $PbZrO_3$," *Chem. Mater.*, **17**, 4594–4599 (2005).
11. W. Zhu, Z. Wang, C. Zhao, et al., "Low temperature processing of nanocrystalline lead zirconate–titanate (PZT) thick films and ceramics by a modified sol-gel route," *J. Appl. Phys.*, **41**, 6969–6975 (2002).
12. A. Banerjee and S. Bose, "Free-standing lead zirconate–titanate nanoparticles: low-temperature synthesis and densification," *Chem. Mater.*, **16**, 5610–5615 (2004).
13. S. Roy, S. Bysakh, and J. Subrahmanyam, "Metastable face-centered cubic lead zirconate-titanate (PZT) and lead lanthanum zirconate–titanate (PLZT) nanocrystals synthesized by autoignition of metal-polymer gel," *J. Mater. Res.*, **23**, No. 3, 719–724 (2008).
14. M. S. Dash, J. Bera, and S. Ghosh, "Study on phase formation and sintering kinetics of $BaTi_{0.6}Zr_{0.4}O_3$ powder synthesized through modified chemical route," *Alloys Compd.*, **430**, 212–216 (2007).
15. R. A. Das, A. Pathak, and P. Pramanik, "Low-temperature preparation of nanocrystalline lead zirconate–titanate and lead lanthanum zirconate–titanate powders using triethanolamine," *J. Am. Ceram. Soc.*, **81**, No. 12, 3357–3360 (1998).
16. Z. Surowiak, M. F. Kupriyanov, and D. Czekaj, "Properties of nanocrystalline ferroelectric PZT ceramics," *J. Eur. Ceram. Soc.*, **21**, 1377–1481 (2001).
17. W. S. Clabaugh, E. M. Swiggard, and R. Gilchrist, "Synthesis of barium titanate from oxalate precursor," *J. Res. Nat. Bur. Stud.*, **56**, No. 5, 289–293 (1956).
18. A. V. Ragulya, O. O. Vasyl'kiv, V. V. Skorokhod, and N. V. Danilenko, "Synthesis and sintering of nanocrystalline barium titanate powder under nonisothermal conditions. IV. Electron microscope study of the evolution of barium titanate powder morphology," *Powder Metall. Met. Ceram.*, **37**, No. 3─4, 137–144 (1998).

19. V. M. Pogibko, V. V. Prisedskii, and I. L. Sidak, “Studying the mechanisms of thermal decomposition of the barium titanate oxalate precursor,” *Vopr. Khim. Khim. Tekhnol.*, No. 1, 110–115 (2010).
20. V. Ischenko, E. Pippel, R. Köferstein, et al., “Barium titanate via thermal decomposition of Ba, Ti-precursor complexes: The nature of the intermediate phases,” *Solid State Sci.*, **9**, 21–25 (2007).
21. V. V. Prisedskii, L. G. Gusakova, and V. V. Klimov, “Initial-stage sintering kinetics of lead zirconate–titanate ceramics,” *Neorg. Mater.*, **12**, No. 11, 1995–1999 (1976).
22. R. L. Coble, “Sintering crystalline solids: II. Experimental test of diffusion models in powder compacts,” *J. Appl. Phys.*, **32**, No. 5, 793–799 (1961).
23. J. R. Grosa, “Nanocrystalline powder consolidation methods,” in: Carl C. Coch (ed.), *Nanostructured Materials: Processing, Properties and Applications*, William Andrew Inc., New York (2007), p. 173–234.